crystals

MDPI

Article

Study on Surface Roughness Improvement of Selective Laser Melted Ti6Al4V Alloy

Di Wang [2], Jiale Lv [2], Xiongmian Wei [2], Dong Lu [1,*] and Chen Chen [1]

[1] State Key Laboratory of Vanadium and Titanium Resources Comprehensive Utilization, Pangang Group Research Institute Co., Ltd., Panzhihua 617000, China
[2] School of Mechanical and Automotive Engineering, South China University of Technology, Guangzhou 510641, China
* Correspondence: ludong_1786@foxmail.com

Abstract: To improve the surface quality of Ti6Al4V parts formed by selective laser melting (SLM), this paper systematically studies the effects of laser power, scanning speed and inclination angle on the different surface morphology and roughness of parts. On this basis, the effect of surface remelting and multi-layer profile scanning process strategies on improving the surface quality of parts is explored. The upper surface roughness varies parabolically with increasing line energy density, the line energy density value that minimizes the upper surface roughness is around 0.22 J/mm, and the minimum Ra value is 4.41 μm. The roughness of upper and lower sides increases significantly with the increase in scanning speed. As the inclination angle increases, the roughness of the upper and lower sides gradually decreases, which is caused by the combined influence of powder adhesion and step effect. The surface remelting process strategy can reduce the upper surface roughness by 35.68% and reduce its Ra value to 2.65 μm. The multi-layer profile scanning process strategy can reduce the upper side and vertical side roughness by more than 50%, down to Ra 5.10 μm and Ra 4.61 μm, respectively.

Keywords: selective laser melting; Ti6Al4V; surface roughness improvement; process parameters; process strategies

Citation: Wang, D.; Lv, J.; Wei, X.; Lu, D.; Chen, C. Study on Surface Roughness Improvement of Selective Laser Melted Ti6Al4V Alloy. *Crystals* **2023**, *13*, 306. https://doi.org/10.3390/cryst13020306

Academic Editors: Liang Lan, Haifeng Yang, Guoxin Lu and Shuang Gao

Received: 11 January 2023
Revised: 8 February 2023
Accepted: 10 February 2023
Published: 13 February 2023

1. Introduction

Additive Manufacturing (AM) technology is a new type of manufacturing technology developed in recent decades. It turns digital models into solid parts through the layer-by-layer stacking of materials, overturning traditional design and manufacturing approaches. AM technology has been widely used in aerospace, rail transportation, new energy, new materials, medical instruments and other industries [1]. Selective Laser Melting (SLM) is one of the most important technologies in the field of metal AM, using high-energy density laser to selectively melt spherical metal powders and form complex metal components with high densities [2]. SLM technology has been widely used in the AM of magnesium-based alloys [3], nickel-based alloys [4], titanium-based alloys [5] and other metals.

Ti6Al4V alloy is an α + β type two-phase titanium alloy with the advantages of low density, high specific strength, good corrosion resistance, good high temperature mechanical properties, being non-toxic and non-magnetic, good heat resistance and good weldability. As a consequence, it is widely used in aerospace, marine, petroleum, chemical and medical industries [6]. The Ti6Al4V alloy has a high absorption rate of laser energy, and its complex components are suitable for forming via SLM technology [7]. However, due to defects such as spheroidization, powder adhesion, and discontinuity of the melting channel on the surface of SLM-formed parts, the surface roughness is poor [8]. Surface roughness is an important characterization parameter of surface quality, and its size affects the wear resistance, fatigue performance and corrosion resistance of the formed part, which in turn

affects the service life of the formed part [9]. Therefore, in order to improve the performance of SLM-formed parts, it is necessary to find a way to reduce the surface roughness.

The surface roughness of SLM-formed Ti6Al4V parts strongly depends on its processing parameters. Li et al. [10] proposed a method based on the Response Surface Methodology (RSM) to improve the surface quality of SLM-formed Ti6Al4V parts. The parameter set is composed of laser power, scanning speed and scanning space, and the optimal parameters are obtained by RSM method collected and verified experimentally. Krol et al. [11] investigated the effects of laser power, scanning speed, scanning space and exposure time on the roughness of the upper and side surfaces of SLM-formed Ti6Al4V specimens using the controlled variable method, and experimentally explored the optimal process parameters. They pointed out that the upper surface roughness is mainly caused by the ripple effect and that the inclined side surface roughness is mainly caused by the step effect and powder adhesion. Han et al. [12] formed Ti6Al4V specimens via SLM using different scanning strategies, and found that lower surface roughness could be obtained using the helical scanning strategy than using the S-shaped scanning strategy, and the roughness of the surface on the side parallel to the scanning direction was lower than that on the side perpendicular to the scanning direction. Sadali et al. [13] investigated the relationship between scanning speed and the surface roughness of SLM-formed Ti6Al4V specimens and found that the surface roughness of formed specimens showed a parabolic trend of increasing and then decreasing as the scanning speed increased, a phenomenon attributed to droplet diffusion kinetics and powder adhesion. Oyesola et al. [14] used the RSM method to predict the optimal values of laser power and scanning speed in response to surface roughness and surface hardness. Xiao et al. [15] investigated the effect of layer-by-layer remelting scanning on the upper surface roughness of SLM-formed Ti6Al4V specimens, and the experiments showed that the higher the remelting laser power, the lower the scanning speed will be, and the smaller the scanning space, the lower the roughness is too. Only the suitable remelting scanning parameters can effectively reduce upper surface roughness. Chen et al. [16] experimentally pointed out that the surface roughness of SLM-formed Ti6Al4V specimens was related to the angle of specimen placement, and the surface roughness of the upper side was lower than that of the lower side due to more severe powder adhesion on the lower side than on the upper side.

It can be seen that the current research on the surface roughness of Ti6Al4V formed by SLM focuses on the exploration of the optimal process parameters. How to further improve the surface quality of parts under good forming parameters should also arouse researchers' thinking. The aforementioned research work of Xiao et al. [15] deserves our attention, but there are still few studies on the process strategies of SLM forming of Ti6Al4V.

This paper conducts process experiments for the purpose of improving the surface quality of parts. We explored the effects of laser power, scanning speed and inclination angle on different surface morphologies and the roughness of parts. Based on this, we studied the effect of surface remelting and multi-layer profile scanning process strategies on the surface quality improvement of parts.

2. Materials and Methods

2.1. Materials and Equipment

The metal powder material used in this experiment is the plasma atomized Ti6Al4V spherical powder, produced by AP&C Company, and its elemental composition is shown in Table 1. It can be seen from the microscopic morphology of the powder in Figure 1a that the sphericity of the Ti6Al4V powder is good. The particle size distribution of the powder is between 15 and 45 μm, and the D_{50} is 23.37 μm. The particle size distribution is shown in Figure 1b.

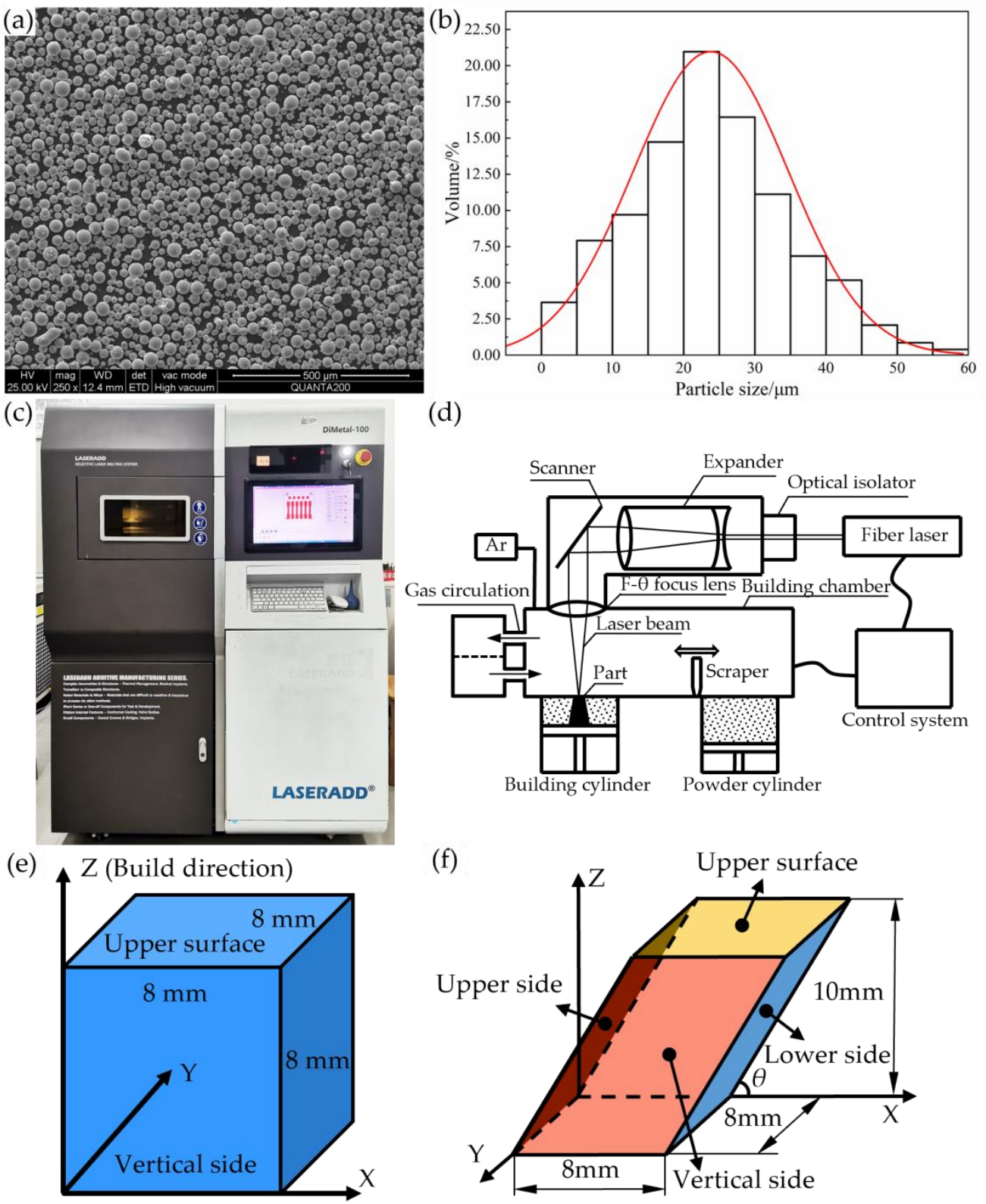

Figure 1. SLM forming model, equipment and powder: (**a**) micro morphology of Ti6Al4V powder; (**b**) particle size distribution; (**c**) the DiMetal-100 forming equipment; (**d**) the technical principles of SLM; (**e**) cube schematic; (**f**) oblique square schematic.

Table 1. Chemical composition of Ti6Al4V powder.

Element	C	O	N	H	Fe	Al	V	Ti
Mass fraction/%	0.02	0.11	0.02	0.0034	0.19	6.5	3.9	bal

The SLM forming equipment used in this paper is the Dimetal-100 forming equipment (Guangzhou LeiJia Additive Manufacturing Technology Co., Ltd., Guangzhou, China) shown in Figure 1c. The maximum forming size of the equipment is 100 mm × 100 mm × 120 mm, and it can be equipped with a fiber laser with a maximum laser power of 500 W. The diameter of the focused spot is 60–80 μm, and the maximum scanning speed is 7.8 m/s. The schematic diagram is shown in Figure 1d.

2.2. Experimental Model

In order to study the effects of process parameters on different surface roughness, the specimens formed in this paper are divided into two types. The cubic block specimen with an 8 mm edge length shown in Figure 1e is used to study the effect of different process parameters on the roughness of the upper surface and the vertical side. A total of 36 samples were formed and measured using parameter set 1 of Table 2. The forming effect is shown in Figure 2a,b. The specimen used to study the relationship between the roughness of the upper and lower side surfaces and different process parameters is the oblique square specimen, shown in Figure 1f, whose bottom surface is a square 8 mm side length and 10 mm in height. The inclination angle of the oblique square is recorded as θ. We took θ as 45°, using parameter set 2 in Table 2 to form and measure 10 samples to explore the influence of different process parameters on the roughness of the upper and lower sides. Taking θ as 25°, 30°, 35°, 40°, 45°, 50°, 60°, 70°, 80° and 90°, respectively, 10 samples were formed and measured using the parameter set 3 of Table 2 to explore the effect of different inclination angles on the roughness of the upper and lower sides. The forming effect is shown in Figure 2c. To explore the effect of surface remelting process on the upper surface roughness, the cube specimens were formed using Table 2 parameter set 4. The upper surface was remelted 2 layers by layer, the only difference between the remelting process parameters and the forming process parameters being the addition of 0.04 mm scanning line offset. To study the effect of multi-layer profile scanning on surface roughness, the same Table 2 parameter, set 4, was used to form the internal solid of the inclined cube specimen with θ of 45°. The scanning speed was reduced to 400 mm/s when scanning the profile line.

2.3. Analysis and Characterization Tools

The formed Ti6Al4V specimens were cleaned with an ultrasonic water bath to exclude the influence of excess powder on the surface roughness measurement results. In the 3D morphological photograph of the specimen surface taken by VHX-5000 ultra-depth 3D microscope, three surface profiles were taken perpendicular to the reference surface in order to calculate the average roughness value. The sampling length of the upper surface and the vertical side is 5 mm, and the sampling length of the upper and lower sides is 8 mm.

Table 2. Forming process parameters.

Process Parameters	Value			
	Parameter Set 1	**Parameter Set 2**	**Parameter Set 3**	**Parameter Set 4**
Scanning speed/(mm/s)	600, 800, 1000, 1200, 1400, 1600	400, 600, 800, 1000, 1200	800	1000
Laser power/W	100, 120, 140, 160, 180, 200	120, 140, 160, 180, 200	160	160
Layer thickness/mm	0.03	0.03	0.03	0.03
Scanning space/mm	0.08	0.08	0.08	0.08

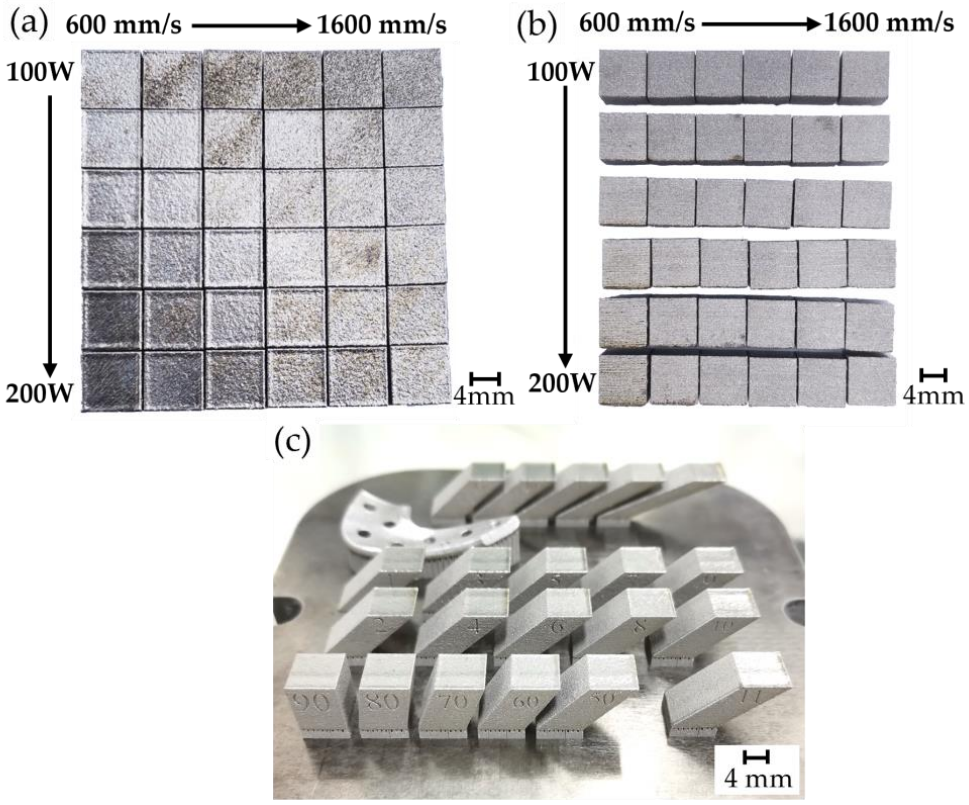

Figure 2. Forming effect of specimens: (**a**) upper surfaces of cube specimens; (**b**) vertical sides of cube specimens; (**c**) oblique square specimens.

For a surface profile of length L, the one-dimensional definition of the arithmetic mean deviation of the profile [17] is:

$$\mathrm{Ra} = \frac{1}{\mathrm{L}}\int_0^{\mathrm{L}} |f(x)|\mathrm{d}x \tag{1}$$

where $f(x)$ represents the deviation between the surface height at x and the midline of the profile, which is calculated by the least squares method of the profile in this paper. The deviation f_n between the surface height and the profile midline is measured at N positions along the profile length L, and the numerical calculation of the surface roughness Ra is simplified as:

$$\mathrm{Ra} \approx \frac{1}{\mathrm{N}}\sum_{n=1}^{\mathrm{N}} |f_n| \tag{2}$$

For a surface profile with length L, the maximum profile height Rz is equal to the distance between the maximum profile peak height f_p and the maximum profile valley depth f_v, namely:

$$\mathrm{Rz} = f_p + f_v \tag{3}$$

In order to make the article more concise, some abbreviations will be used in the article, see Table 3.

Table 3. Abbreviation.

Full Name	Abbreviation
Upper Surface Roughness	USR
Vertical Side Roughness	VSR
Upper Side Surface Roughness	USSR
Lower Side Roughness	LSR
Line Energy Density	LED

3. Results and Discussion

3.1. Variations in Morphology and Roughness of Each Surface under Different Parameters

3.1.1. Upper Surface

As shown in Figure 3a, at the same laser power, the USR tends to increase gradually, or otherwise decrease first and then increase with the increase in the scanning speed. Taking the laser power of 180 W as an example, as shown in Figure 4, at the scanning speed of 600 mm/s, there are slight undulations as well as outer edge bulges on the upper surface; at the scanning speed of 1000 mm/s, the upper surface is relatively flat, with only a small amount of spatter particles; at the scanning speed of 1400 mm/s, obvious local depressions and spheroidized bulges are observed on the upper surface.

According to Figure 3b, the USR shows a decreasing trend with the increase in laser power at most scanning speeds. When the scanning speed is only 600 mm/s, the USR first decreases and then increases. As shown in Figure 4, with the increase in laser power, at the scanning speed of 1400 mm/s, the depression and spheroidization on the upper surface decreased continuously, and finally only a small amount of spatter particles were embedded in it. While at the scanning speed of 600 mm/s, the upper surface undulations gradually eased while the ripple-like bulges became obvious. It was also observed that the outer edge bulge phenomenon on the upper surface became more and more obvious with the increase in laser power, and the affected area was expanded.

From the above results, it can be seen that the upper surface quality of the parts at lower scanning speed is generally better. However, at certain laser power, low scanning speed instead increases the roughness. Higher scanning speed will lead to concave and convex parts surface, when increasing the laser power can effectively reduce the roughness. Therefore, the USR is affected by the combination of scanning speed and laser power, and the ratio of laser power to scanning speed, i.e., the line energy density (LED), is used to quantify this effect. When the LED is higher, the laser melts more metal powder, the molten metal liquid has good wettability, inhibits the appearance of spheroidization, and the formed melting channel is regular and continuous, which makes the USR lower. However, too high a LED can easily lead to overburning and outer edge bulge phenomena, which deteriorate the surface quality. When the LED is low, the laser input energy is not enough, the powder cannot be fully melted and spread, the formed melting channel is not continuous or even raised, and the lap forms an undulating surface shape, which increases the USR.

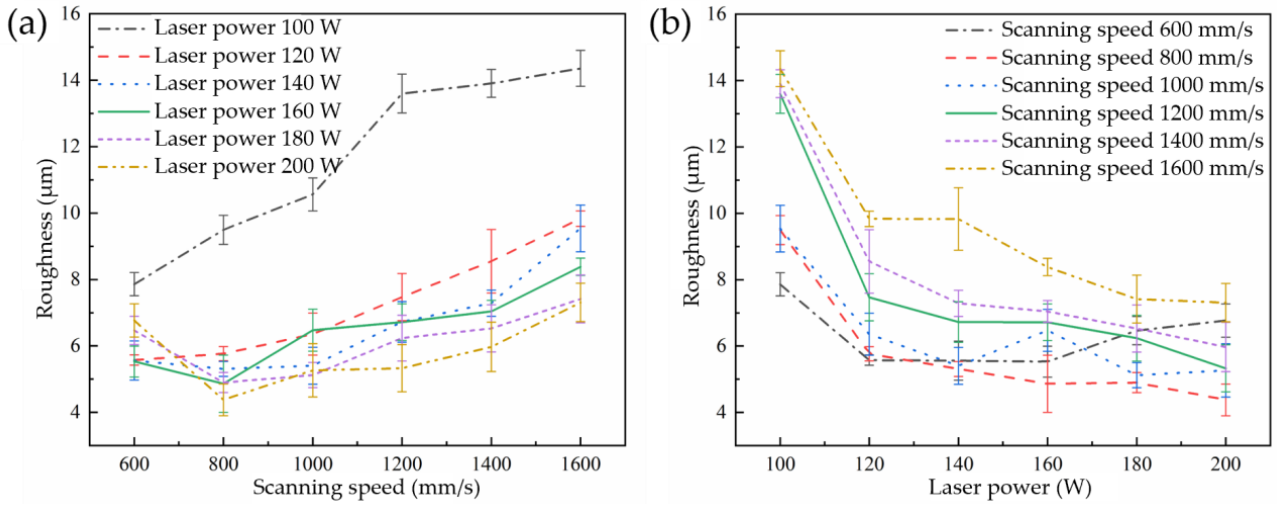

Figure 3. USR under different parameters: (**a**) scanning speed; (**b**) laser power.

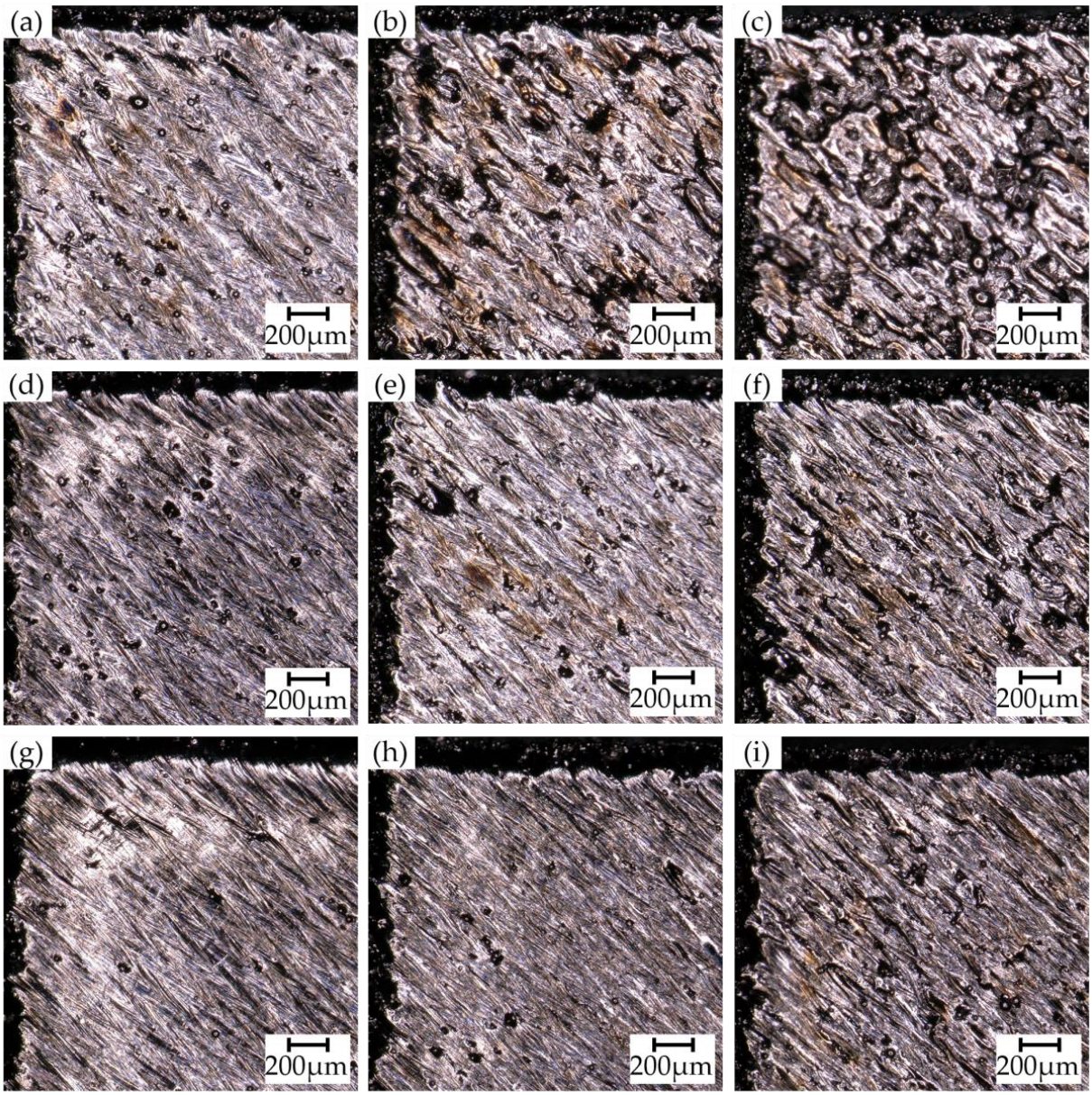

Figure 4. Upper surface morphology under different parameters: (**a**) 100 W, 600 mm/s; (**b**) 100 W, 1000 mm/s; (**c**) 100 W, 1400 mm/s; (**d**) 140 W, 600 mm/s; (**e**) 140 W, 1000 mm/s; (**f**) 140 W, 1400 mm/s; (**g**) 180 W, 600 mm/s; (**h**) 180 W, 1000 mm/s; (**i**) 180 W, 1400 mm/s.

Figure 5 shows the LED when forming each specimen. The LED corresponding to the minimum roughness of the upper surface under the same laser power is marked by the blue line frame. It can be seen that under different laser powers, the LED corresponding to the minimum roughness is different. The laser power increases from 140 W to 200 W, and the LED corresponding to the minimum roughness gradually increases. This shows that the energy density alone is not enough to fully reflect the influence of laser power and scanning speed on the surface roughness. Under different laser power levels, the LED to be used should be different. From the perspective of the change trend, the LED value to obtain the minimum USR is around 0.22 J/mm, and the minimum Ra value is 4.41 μm. The higher the laser power, the greater the required LED, that is, a lower scanning speed is required. The reason is that the solidification state of the molten pool is different under the same energy density and different scanning speeds. At high scanning speeds, the laser irradiation time of the powder is short, the molten pool solidifies rapidly, and it is easier to produce spheroidization. Therefore, the USR changes in a parabola as the LED increases,

and the position of the lowest point of the parabola depends on different laser powers. The higher the laser power, the greater the LED at the lowest point. The process parameters to minimize the roughness of the upper surface are: laser power 200 W, scanning speed 800 mm/s, Sadali et al. [10] obtained similar data. When the laser power is 100 W and 120 W, the roughness continues to increase with the increase in the scanning speed, because the roughness is in the rising part of the parabola.

Laser power/W \ Scanning speed/(mm/s)	600	800	1000	1200	1400	1600
100	0.17	0.13	0.10	0.08	0.07	0.06
120	0.20	0.15	0.12	0.10	0.09	0.08
140	0.23	0.18	0.14	0.12	0.10	0.09
160	0.27	0.20	0.16	0.13	0.11	0.10
180	0.30	0.23	0.18	0.15	0.13	0.11
200	0.33	0.25	0.20	0.17	0.14	0.13

Figure 5. LED during the forming process of each specimen(J/mm).

The main factors affecting the USR include spatter behavior, outer edge bulges, and bulges and depressions caused by spheroidization. Spatter is an unavoidable phenomenon in the SLM forming process, including the powder spatter formed by the metal powder escaping the powder bed under the action of gas entrainment and the droplet spatter formed by the escaped molten pool melt or the powder spatter undergoing sputtering and condensation under thermal radiation [18]. On the regular and continuous upper surface of the melting channel, the spatter behavior is the main factor affecting its surface roughness. The outer edge bulge is caused by too short laser on delay or too long laser off delay, which causes the laser to irradiate the powder bed for too long, the energy absorption at the end of the scanning line is too large, and the molten pool increases. At the same time, the end of the scanning line is more exposed to metal powder than other places, and the inhalation of the metal powder by the molten pool further increases the melting width and melting height at the endpoint of the scanning line, thereby forming an outer edge bulge. Cooperative control of laser delay and scanner delays to make them suitable for well-defined jump speed and mark speed can effectively solve the problem of outer edge bulge [19]. Laser energy density is an important factor affecting the spheroidization phenomenon, so choosing an appropriate linear energy density is the key to ensuring the quality of the upper surface.

3.1.2. Vertical Side

From Figure 6a, it can be seen that the VSR of the specimen shows different changes with the change of scanning speed at different laser powers. With the increase in scanning speed, the roughness increases slightly at low laser power; the roughness fluctuates within a certain range at medium laser power; and the roughness decreases continuously at high laser power. From Figure 6c–f, it can be seen that at low laser power, the vertical side of the specimen is completely covered by the adhered powder particles and interspersed with some spheroidized bulges. With the increase in the scanning speed, there is no obvious change in the morphology of the vertical side. At high laser power, when the scanning speed is small, the vertical side is scattered with more lumpy bulges in addition to a large amount of adhered powder; when the scanning speed is high, the vertical side shows a mixture of spheroidized bulges and powder adhesion.

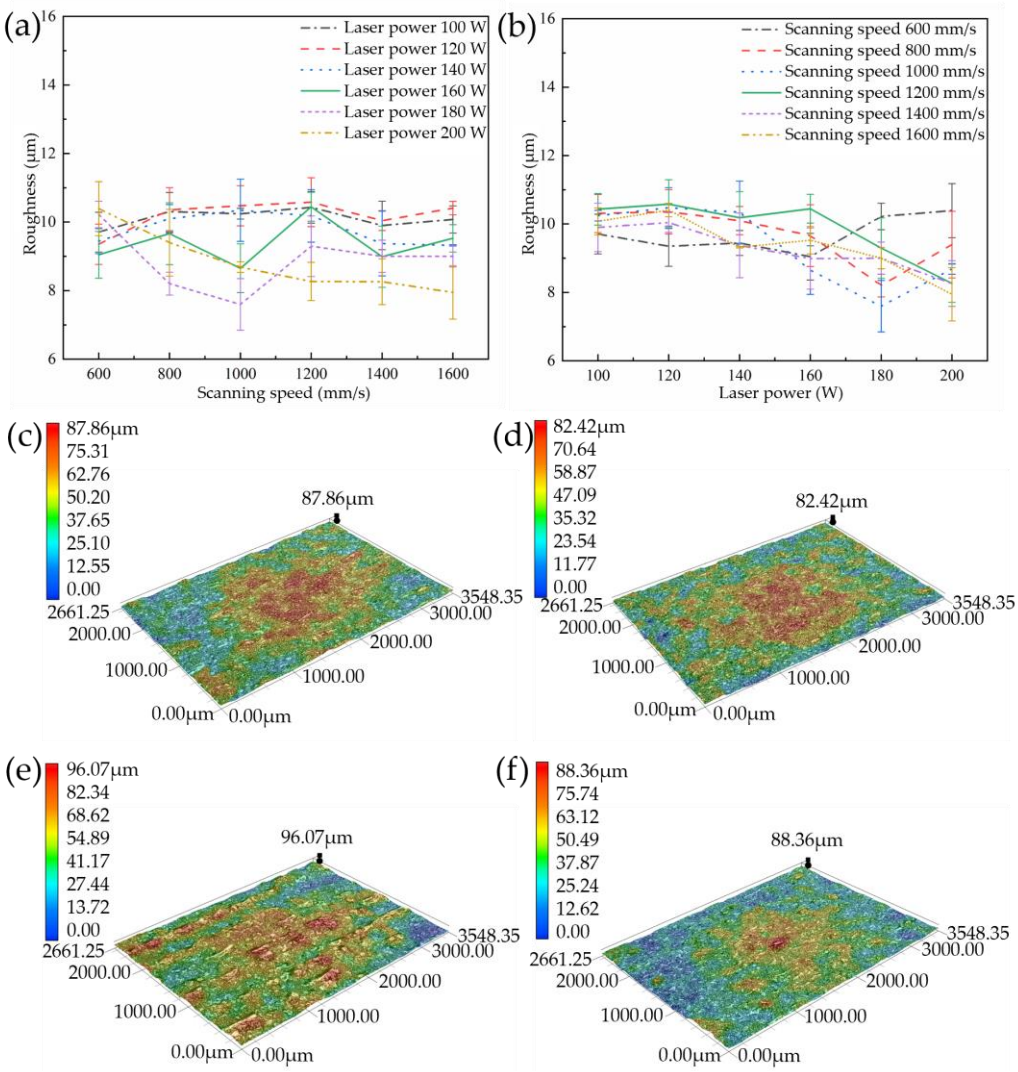

Figure 6. Morphology and roughness of vertical side under different parameters: (**a**) scanning speed; (**b**) laser power; (**c**) 100 W, 600 mm/s; (**d**) 100 W, 1600 mm/s; (**e**) 200 W, 600 mm/s; (**f**) 200 W, 1600 mm/s.

It can be seen from Figure 6b that under different scanning speeds, the VSR has little difference at low laser power, but changes greatly at high laser power. When the scanning speed is 600 mm/s, as the laser power increases, the number of vertical side lumpy bulges increases (Figure 6e), and the roughness tends to increase. When the scanning speed is 1200 mm/s, the roughness decreases continuously with the increase in laser power, and

the surface morphology has no obvious change (Figure 6f). This shows that increasing the laser power will aggravate the spheroidization of the vertical side of the part, resulting in lumpy bulges, and the lower the scanning speed, the greater the effect.

As shown in Figure 7, due to the orthogonal scanning strategy, the scanning line and the vertical side make a certain angle. The melting channel will form a bump at the end after lapping each other, and due to the layer-by-layer stacking of the outer edge bulges, the vertical side becomes concave and uneven. The depressed position tends to gather powder particles and intensify the powder adhesion on the surface, thus forming a vertical side profile with a raised surface and covered with powder particles, and the VSR is thus larger. At higher scanning speed and lower laser power, the laser input energy to the powder bed is limited, the melt pool formed is smaller, the melting channel width is narrower. After the narrow melting channels lap each other, the bump formed on the vertical side is lower, so the roughness is basically unchanged.

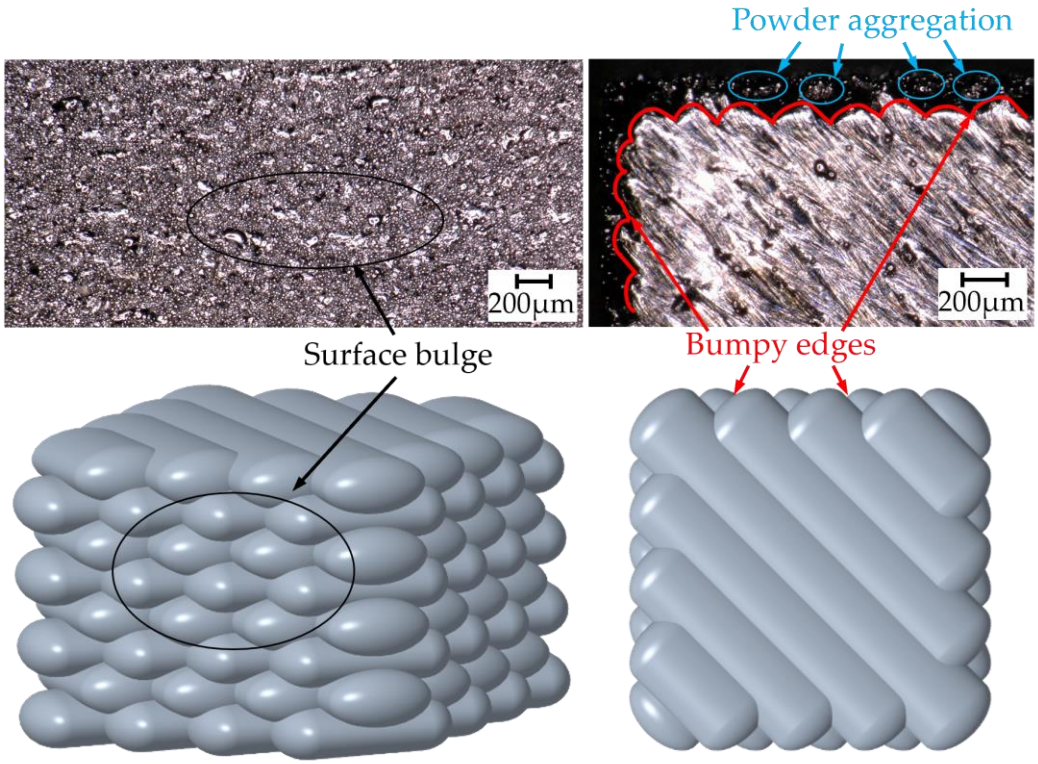

Figure 7. Schematic diagram of vertical side surface topography.

3.1.3. Upper Side

The USSR increased significantly with the increase in scanning speed at the laser power of 160 W (Figure 8a). The increase in scanning speed from 400 mm/s to 1200 mm/s increases Ra by 42.65% and Rz by 56.13%. Analysis of Figure 8c,d shows that the spheroidized bulges on the upper surface gradually evolve into bar bulges as the scanning speed increases, and the length and height of the bar bulges gradually increase, leading to a rapid increase in roughness.

When the scanning speed is 800 mm/s, as the laser power increases, the USSR shows a trend of decreasing with small fluctuations (Figure 8b). Observing Figure 8e,f, the upper side surface under different laser powers is mainly composed of adhered powder particles and bar bulges, with little difference in morphology. When the scanning speed is constant, changing the laser power will not have a significant impact on the USSR.

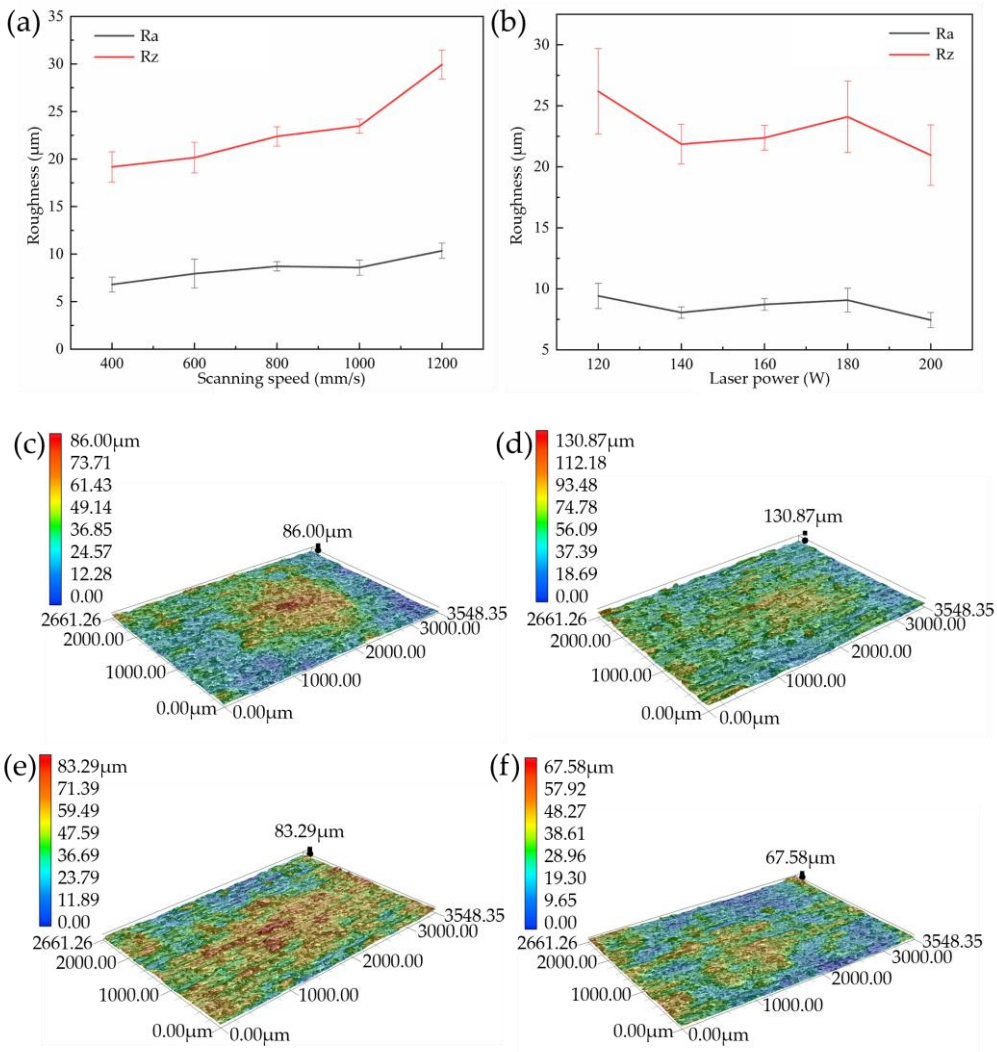

Figure 8. Morphology and roughness of upper side under different parameters: (**a**) scanning speed; (**b**) laser power; (**c**) 160 W, 400 mm/s; (**d**) 160 W, 1200 mm/s; (**e**) 120 W, 800 mm/s; (**f**) 200 W, 800 mm/s.

Figure 9a,b shows the forming effect and roughness curves of the upper side under different inclination angles. The inclination angle increases from 25° to 90°, and the USSR gradually decreases. It can be seen from Figure 9c,d that as the inclination angle increases, the powder adhered to the upper side increases continuously, and the continuous blocky entities part is gradually covered by loose powder particles.

According to the above results, it can be seen that the upper side morphology and roughness are mainly determined by the intensity of the unfused powder adhering to the step edge and the geometry of the step edge (Figure 10a). As shown in Figure 10b, during the laser melting of the powder, the heat at the edge of the step comes from thermal diffusion, which is not enough to completely melt the powder particles, and the unmelted powder particles tend to adhere to the step edge, causing the powder adhesion phenomenon [20]. As the inclination angle increases, the step edges of adhered powder particles approach each other, resulting in a higher concentration of adhered powder particles on the upper side (Figure 9d). The main factor affecting the geometry of the step edge is the step effect. As shown in Figure 10c, the upper side will produce a step effect after discrete slicing, resulting in the deviation between the actual profile and the theoretical profile of the formed specimen. As the inclination angle increases, the height difference between the lowest point of the step and the theoretical profile decreases, the distance between the apexes of the steps also decreases, and the step effect weakens. Therefore, with

the increase in the inclination angle, under the comprehensive influence of the powder adhesion phenomenon and the step effect, the unevenness of the upper side gradually changes from a wide and high peak to a narrow and low peak, so that the roughness gradually decreases.

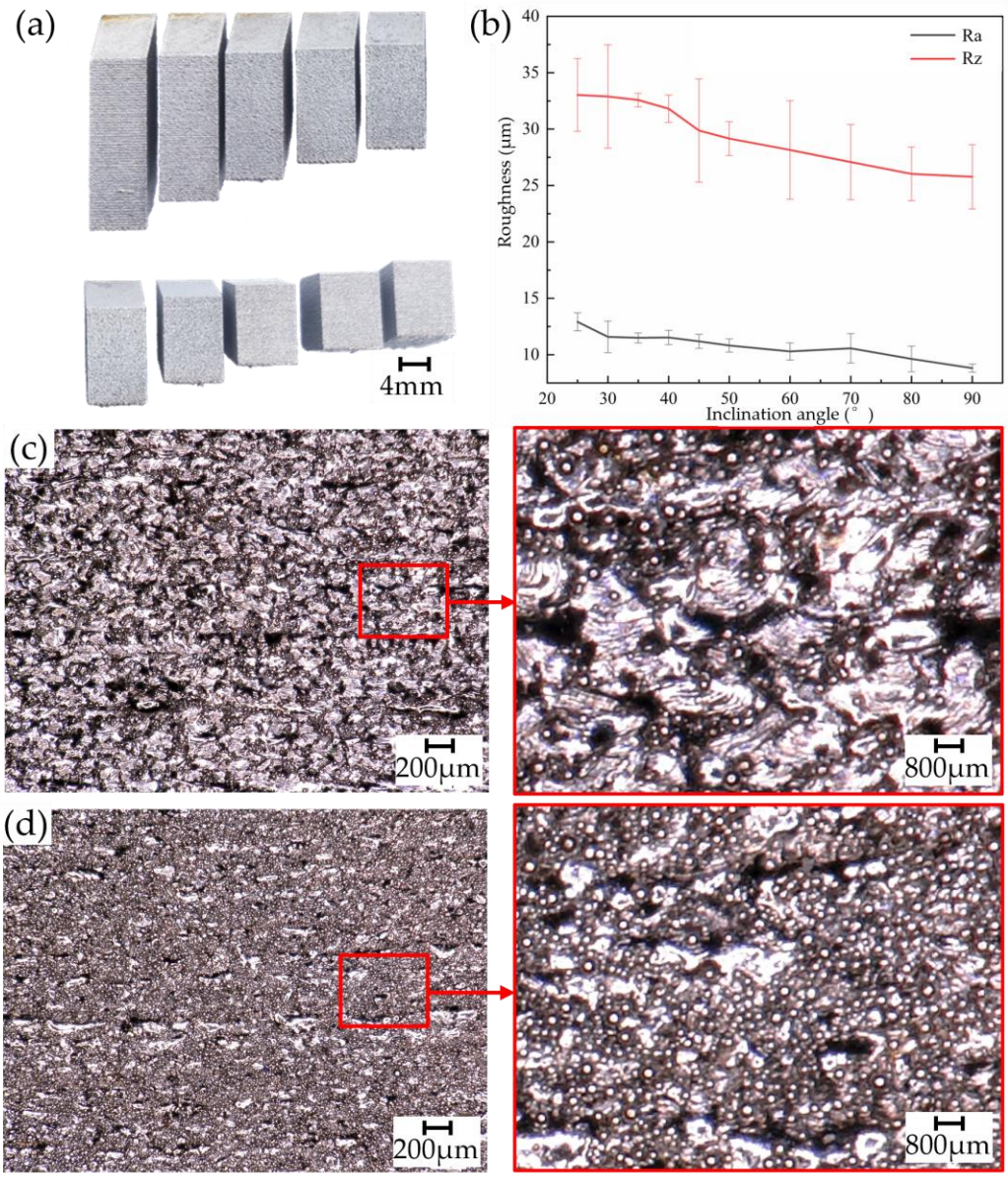

Figure 9. Upper side of parts with different inclination angles: (**a**) forming effect; (**b**) roughness curve; (**c**) 25° macroscopic morphology; (**d**) 90° macroscopic morphology.

3.1.4. Lower Side

As shown in Figure 11a, the LSR of the specimen increased rapidly with the increase in the scanning speed at the laser power of 160 W. The scanning speed increases from 400 mm/s to 1200 mm/s, and Ra increases from 11.18 μm to 23.75 μm, an increase of 112.43%. Rz also increases from 26.89 μm to 57.68 μm, an increase of 114.50%. This shows that the scanning speed has a great influence on the LSR at this laser power. As seen in Figure 11c,d, with the increase in scanning speed, the powder particles adhered to the lower side gradually increased, and the blocky entities gradually decreased and appeared to be raised, so the roughness increased exponentially.

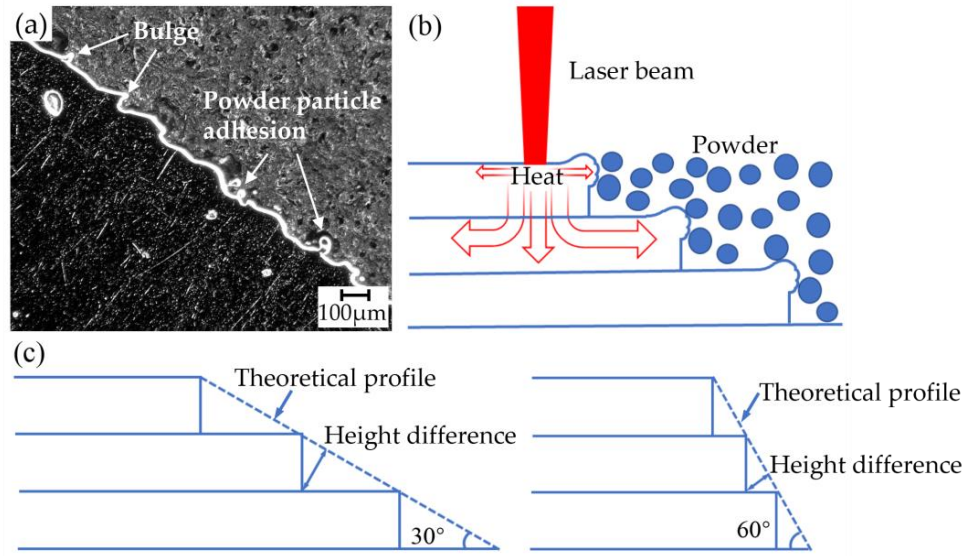

Figure 10. Typical morphology and principle of the upper side during SLM: (**a**) section diagram; (**b**) schematic diagram of thermal diffusion; (**c**) step effect.

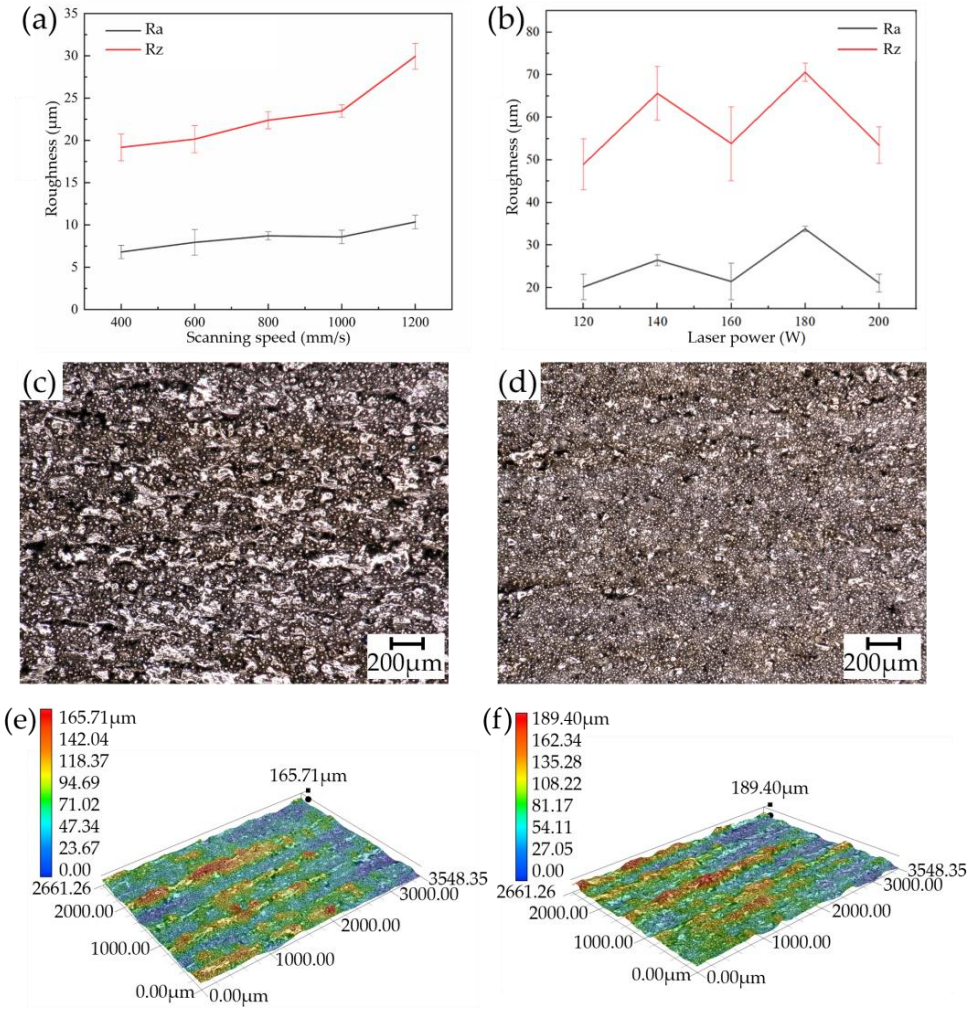

Figure 11. Morphology and roughness of lower side under different parameters: (**a**) scanning speed; (**b**) laser power; (**c**) 160 W, 400 mm/s; (**d**) 160 W, 1000 mm/s; (**e**) 120 W, 800 mm/s; (**f**) 200 W, 800 mm/s.

As shown in Figure 11b, with the increase in laser power, the LSR of the specimen showed a fluctuating trend of change. It can be seen that at the scanning speed of 800 mm/s, there is no direct relationship between the laser power and the LSR, and smaller surface roughness can be obtained at high or low laser power. This is confirmed by the 3D morphology of the lower side shown in Figure 11e,f, where there are serious powder adhesion and some bar bulges on the lower side at different laser powers, with little difference in the height of the bulges and no obvious change in the macroscopic morphology.

Figure 12a,b shows the forming effect and roughness curves of the lower side under different inclination angles. It is found that with the continuous increase in the inclination angle, both Ra and Rz decrease rapidly, and when the inclination angle is greater than 40°, the rate of decline slows down. When the inclination angle increased from 25° to 35°, the angle only changed by 10°, but Ra decreased by 48.24%. When the inclination angle increases from 40° to 90°, the Ra value only decreases by 52.09%. When the inclination angle is within 40°, the Ra of the lower side is greater than 20 μm. When the inclination is 20°, the Ra even reaches 46.50 μm, and the Rz exceeds 100 μm. It can be seen that the unevenness of the lower side is very large. When the inclination angle was 25°, the lower side of the specimen was basically covered by loose powder particles, which contained a small amount of small blocky entities (Figure 12c). As the inclination angle increases, the lower side gradually becomes dominated by scattered blocky entities, the number of adhered powder particles decreases, and the surface undulation gradually decreases (Figure 12d).

From the above results, it can be seen that when the inclination angle is within 40°, a large number of adhered powder particles and surface undulations jointly lead to poor quality and high roughness of the lower side. When the inclination angle is above 40°, as the inclination angle increases, the surface morphology of the lower side tends to be consistent, the amount of sticky powder is continuously reduced, and the surface fluctuation is continuously reduced, so that the surface quality continues to improve and the surface roughness continues to decrease. The morphology of the lower side is mainly determined by the solidification profile, powder adhesion and step effect. As shown in Figure 13, a step effect will appear after the lower side is sliced, and the smaller the inclination angle is, the larger the hanging area between layers will be. While the hanging area lacks a solid matrix and the melt pool is supported by loose powder. The melt pool penetrates downward under the effect of powder capillary forces and the gravity of the melt pool, which in turn leads to a further increase in the depth and width of the melt pool due to the small thermal conductivity of the powder particles, a phenomenon also known as the laser deep penetration effect [21,22]. The larger size of the melt pool that is trapped into the powder bed will contact more powder, and the forming surface will experience severe powder adhesion, slagging, and larger bulges due to thermal diffusion [23].

3.2. Surface Quality Improvement Process

3.2.1. Effect of Remelting Process Strategy on the Upper Surface

As shown in Figure 14a,b, wavy melting channels and many spatter particles of different sizes can be observed on the original upper surface without remelting. The spatter particles on the upper surface after remelting are significantly reduced, the wavy melting channel projection is significantly improved, and the boundary between the melting channels becomes less obvious. Figure 14c is the profile curve of the section perpendicular to the scanning direction before and after remelting, and the comparison reveals that: the undulation of the no remelting surface is large, with high crest and deep trough, while the peak height and width of the remelting surface decrease. Measuring the surface roughness before and after remelting shows that the Ra of the no remelting surface is 4.12 μm, while the Ra of the remelting surface is 2.65 μm, a decrease of 35.68%. It can be seen that the remelting process strategy can effectively improve the surface quality of the upper surface of the specimen and reduce the surface roughness.

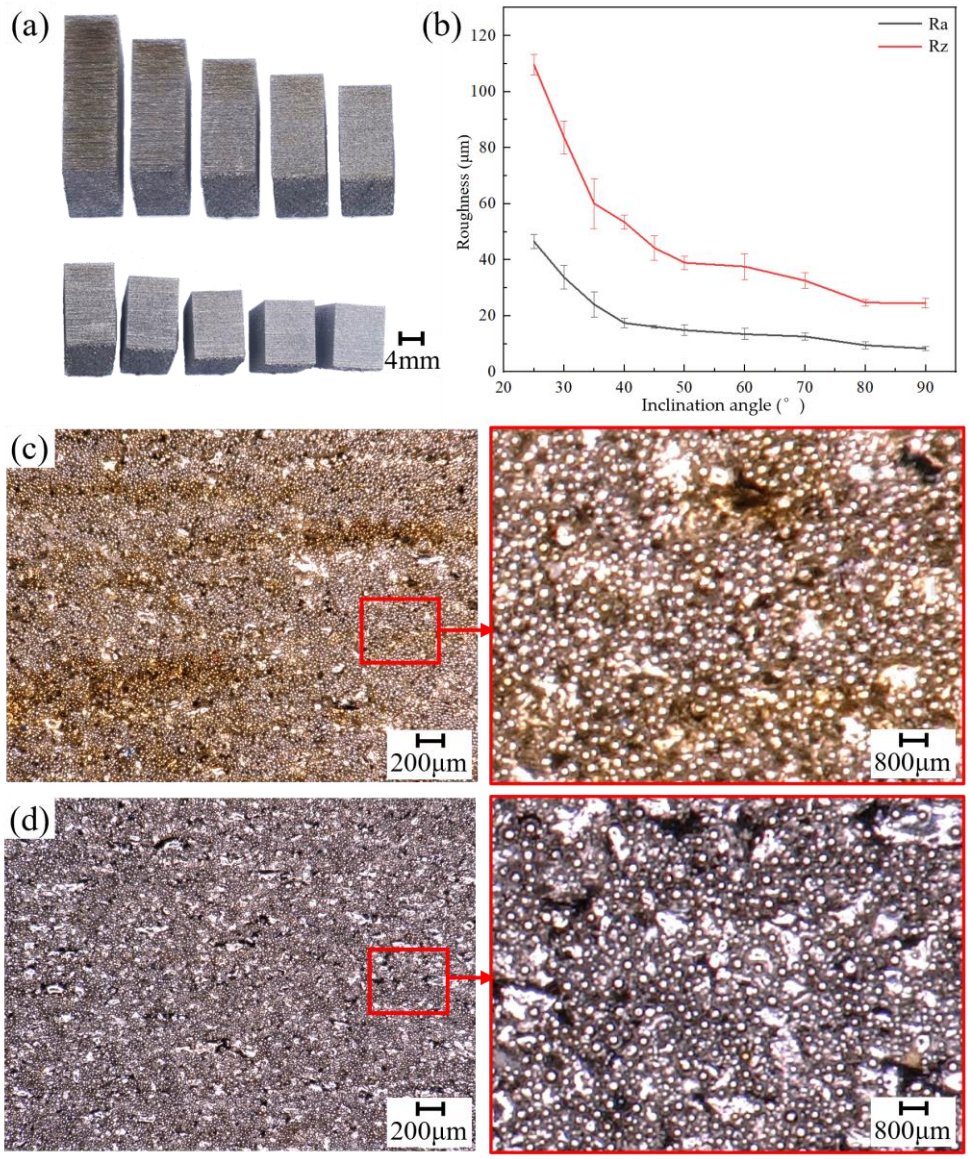

Figure 12. Lower side of parts with different inclination angles: (**a**) forming effect; (**b**) roughness curves; (**c**) 25° macroscopic morphology; (**d**) 90° macroscopic morphology.

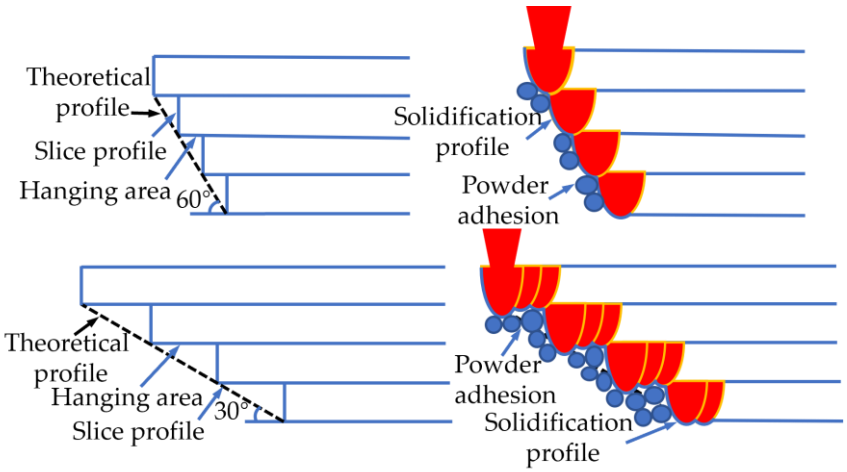

Figure 13. Diagram of forming the lower side surface topography.

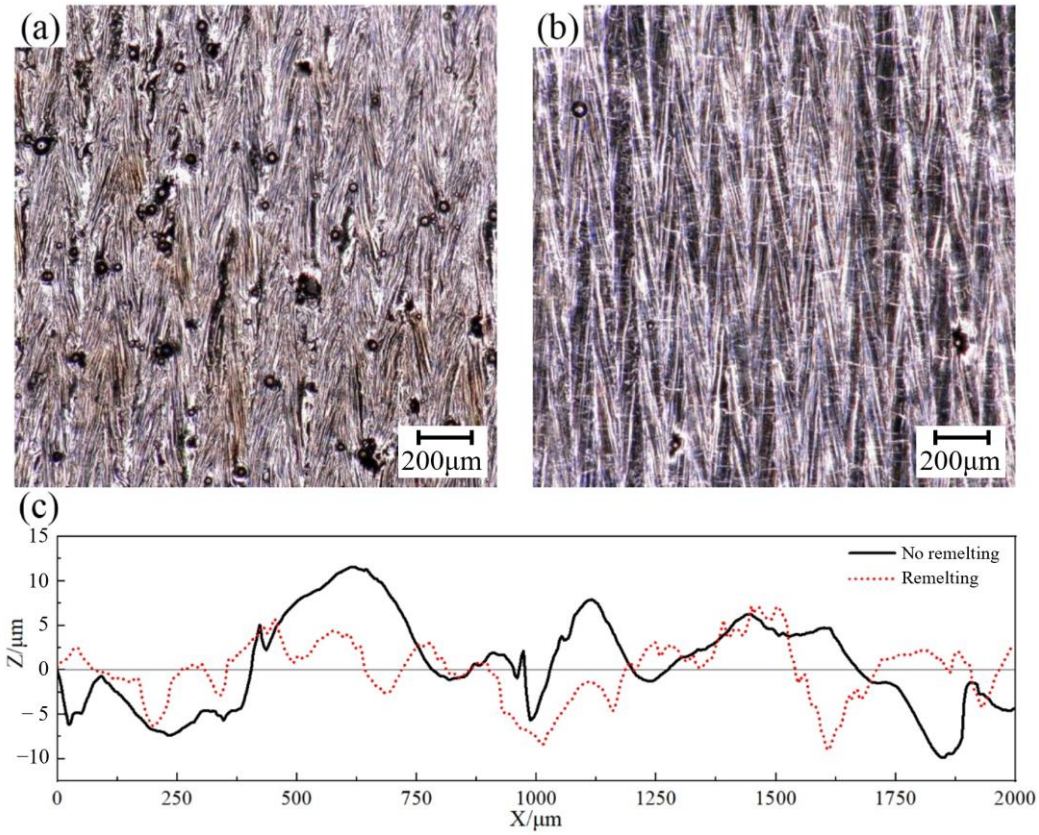

Figure 14. Macroscopic morphology of upper surface before and after remelting: (**a**) no remelting; (**b**) remelting; (**c**) comparison of surface profile curves.

The remelting process strategy is to use the laser to scan again when a layer has been formed by laser scanning. Since no new powder is spread, the laser only acts on the freshly formed surface, and the spatter particles adhering to the upper surface and bulges are heated and melted and solidified to form a new melting channel. A temperature gradient exists between the laser-irradiated melting region and the previously solidified region, and the newly melting material also forms a Marangoni convection phenomenon, causing material flow and forming a new upper surface [24]. The partially melting material flows from the crest to the trough under the combined effect of capillary forces and weight [25]. As a result, the quality of the remelting upper surface is improved and the roughness is significantly reduced.

3.2.2. Impact of Multi-Layer Profile Scanning Strategy on the Surface

The schematic diagram of multi-layer profile scanning is shown in Figure 15a, and the variation curves of roughness of upper side, vertical side and lower side with different number of profile scanning layers are shown in Figure 15b. As the number of layers of profile scanning increases, the overall roughness of the upper and vertical sides tends to decrease, and the Ra values can be reduced by more than 50% after scanning a certain number of layers of profile compared with no scanning of profile, down to Ra 5.10 μm and Ra 4.61 μm, respectively. The change of roughness of the lower side is different from that of the upper and vertical sides. When the profile is not scanned, the Ra value of the lower side is higher, and after scanning 1 layer of profile, Ra decreases rapidly, and the roughness keeps increasing by continuing to increase the number of layers of profile scanning. However, the roughness falls back after scanning 5 layers of profile. From Figure 15c–f, when the profile is not scanned, there are many bulges on the lower side, and a large number of powder particles adhere to it. After scanning the profile of 1 layer, the number of bulges on the lower side is significantly reduced. Continuing to increase

the number of profile scanning layers, the height difference of the surface undulations on the lower side gradually increases. When scanning the profile of four layers, the height difference increases from 71.75 μm when scanning the profile of one layer to 106.57 μm. When scanning the 5 layers profile, the lower side is relatively flat as a whole, with only a small number of bulges, and the height difference of the surface undulations is also reduced. Therefore, the surface roughness begins to decrease again.

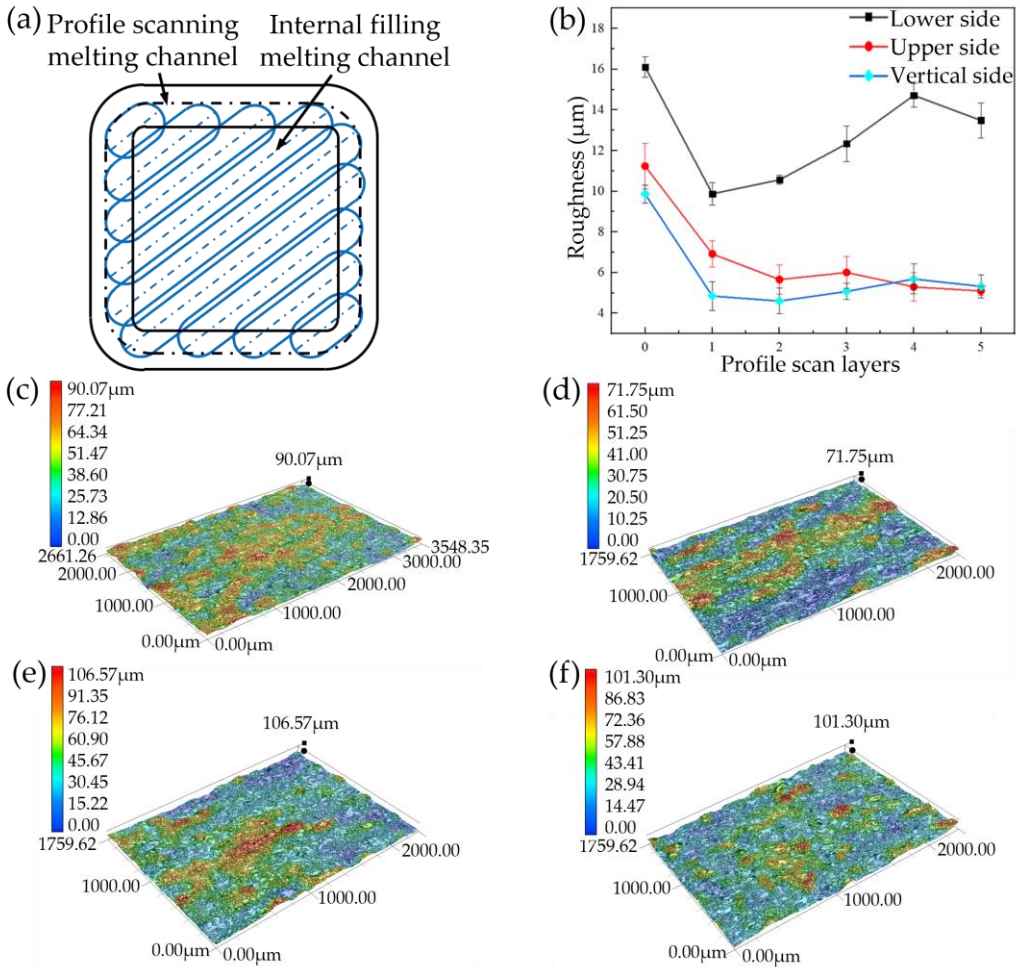

Figure 15. Changes in surface topography and roughness under different profile scanning layers: (**a**) schematic diagram of profile scanning; (**b**) roughness changes; (**c**) lower side of 0 layer; (**d**) lower side of 1 layer; (**e**) lower side of 4 layer; (**f**) lower side of 5 layer.

The reason for the above phenomenon is that, when the profiles are not scanned, the internal filling melting channels lap each other and cause unevenness on the side surfaces. As such, the roughness of both the upper and lower sides as well as the vertical sides is larger at first. Among them, the lower side has the largest surface roughness because the forming surface has no solid substrate and is prone to warpage and slag hanging problems [20]. After scanning the profile of a layer, the profile scanning melting channel covers the edge area of each forming layer, eliminating the depression formed by the overlapping of single melting channels, and the edge shape is more regular and smoother, so the roughness of each side is rapidly reduced. Due to the lower scanning speed used for profile scanning, the laser energy input to the powder bed is high, and the thermal conductivity of the metal powder is much lower than that of the solid metal [26], leading to the accumulation of heat and thus the formation of an excessive melt pool, which aggravates the slagging and powder adhesion phenomena on the lower side [27]. Therefore, continuing to increase the number of profile scanning layers, the roughness of the lower side continues to increase. However, for the upper and vertical sides, the forming

surface is located on the solid substrate. The solid material will conduct and diffuse the heat rapidly, which reduces the heat accumulation caused by multi-layer profile scanning and heat propagation to the surrounding powder. The powder melting and solidification process is fast and stable, and it is less likely to have spattering and irregular edges [28], and so the surface bulge is comparably less and the roughness gradually decreases.

In summary, multi-layer profile scanning can significantly reduce the side roughness of the specimen and improve the surface quality. The number of profile scanning layers has different effects on improving the roughness of different surfaces. The more layers of profile scanning, the lower the roughness of the upper side, while the vertical side has the lowest roughness when scanning the 2-layer profile, and the lower side has the lowest roughness when scanning the 1-layer profile.

4. Conclusions

In this paper, the effects of different laser power, scanning speed and inclination angle on the top surface, vertical side, upper side and lower side of the specimen are analyzed. On this basis, the effect of surface remelting and multi-layer profile scanning on the improvement of surface quality is analyzed. The main conclusions are as follows:

(1) The USR changes in a parabola with the increase in the LED. The position of the lowest point of the parabola depends on different laser powers. The higher the laser power, the greater the LED at the lowest point. The LED value that minimizes the USR is around 0.22 J/mm. The optimal process parameters are laser power 200 W, scanning speed 800 mm/s.

(2) At low laser power, the difference in VSR at different scanning speeds is small; at high laser power, the difference is large. The reason for this is due to the scanning strategy and the outer bulge phenomenon. When the laser power is 160 W, the roughness of the upper and lower sides increases significantly with the increase in scanning speed.

(3) As the inclination angle increases, the USSR gradually decreases due to the weakening of the step effect. Due to serious powder adhesion and slag hanging on the lower side, the roughness is very large at low inclination angles. As the inclination angle increases, the roughness decreases gradually.

(4) The surface remelting process strategy results in a significant reduction in surface roughness due to the attenuation of waviness and spatter on the upper surface. The multi-layer profile scanning process strategy can effectively reduce the roughness of the specimen side surface. The number of profile scanning layers has different effects on improving the roughness of different side surfaces. The more the number of scanning layers, the lower the roughness of the upper side. The vertical side roughness is the lowest when scanning the 2-layer profile, and the lower side has the lowest roughness when scanning the 1-layer profile.

Author Contributions: Writing—original draft preparation, J.L. and X.W.; writing—review and editing, D.W., D.L. and C.C. All authors have read and agreed to the published version of the manuscript.

Funding: This research was funded by the State Key Laboratory of Vanadium and Titanium Resources Comprehensive Utilization, grant number 2021P4FZG11A and the Basic and Applied Basic Research Foundation of Guangdong Province, grant number 2022B1515020064.

Data Availability Statement: Not applicable.

Conflicts of Interest: The authors declare no conflict of interest.

References

1. Lu, B. Additive manufacturing—Current situation and future. *China Mech. Eng.* **2020**, *31*, 19. [CrossRef]
2. Yang, Y.; Chen, J.; Song, C.; Wang, D.; Bai, Y. Current status and progress on technology of selective laser melting of metal parts. *Laser Optoelectron. Prog.* **2018**, *55*, 011401. [CrossRef]
3. Ahmadi, M.; Tabary, S.B.; Rahmatabadi, D.; Ebrahimi, M.; Abrinia, K.; Hashemi, R. Review of selective laser melting of magnesium alloys: Advantages, microstructure and mechanical characterizations, defects, challenges, and applications. *J. Mater. Res. Technol.* **2022**, *19*, 1537–1562. [CrossRef]

4. Abedi, H.; Hanzaki, A.Z.; Azami, M.; Kahnooji, M.; Rahmatabadi, D. The high temperature flow behavior of additively manufactured Inconel 625 superalloy. *Mater. Res. Express* **2019**, *6*, 116514. [CrossRef]
5. Urlea, V.; Brailovski, V. Electropolishing and electropolishing-related allowances for powder bed selectively laser-melted Ti-6Al-4V alloy components. *J. Mater. Process. Technol.* **2017**, *242*, 1–11. [CrossRef]
6. Junfeng, L.; Zhengying, W.; Bingheng, L. Research progress on technology of selective laser melting of titanium and titanium alloys. *Laser Optoelectron. Prog.* **2018**, *55*, 011403. [CrossRef]
7. Brandau, B.; Da Silva, A.; Wilsnack, C.; Brueckner, F.; Kaplan, A.F. Absorbance study of powder conditions for laser additive manufacturing. *Mater. Des.* **2022**, *216*, 110591. [CrossRef]
8. Wang, D.; Wu, S.; Bai, Y.; Lin, H.; Yang, Y.; Song, C. Characteristics of typical geometrical features shaped by selective laser melting. *J. Laser Appl.* **2017**, *29*, 022007. [CrossRef]
9. Uddin, M.; Santifoller, R.; Hall, C.; Schlaefer, T. A Grinding-Burnishing Approach to Enhancing Surface Integrity, Tribological, and Corrosion Behavior of Laser-Cladded AISI 431 Alloys. *J. Manuf. Sci. Eng.* **2022**, *144*, 071003. [CrossRef]
10. Li, Z.; Kucukkoc, I.; Zhang, D.Z.; Liu, F. Optimising the process parameters of selective laser melting for the fabrication of Ti6Al4V alloy. *Rapid Prototyp. J.* **2018**, *24*, 150–159. [CrossRef]
11. Krol, M.; Tański, T. Surface quality research for selective laser melting of Ti-6Al-4V alloy. *Arch. Metall. Mater.* **2016**, *61*, 945–950. [CrossRef]
12. Han, J.; Wu, M.; Ge, Y.; Wu, J. Optimizing the structure accuracy by changing the scanning strategy using selective laser melting. *Int. J. Adv. Manuf. Technol.* **2018**, *95*, 4439–4447. [CrossRef]
13. Sadali, M.F.; Hassan, M.Z.; Ahmad, F.; Yahaya, H.; Rasid, Z.A. Influence of selective laser melting scanning speed parameter on the surface morphology, surface roughness, and micropores for manufactured Ti6Al4V parts. *J. Mater. Res.* **2020**, *35*, 2025–2035. [CrossRef]
14. Oyesola, M.; Mpofu, K.; Mathe, N.; Fatoba, S.; Hoosain, S.; Daniyan, I. Optimization of selective laser melting process parameters for surface quality performance of the fabricated Ti6Al4V. *Int. J. Adv. Manuf. Technol.* **2021**, *114*, 1585–1599. [CrossRef]
15. Xiao, Z.; Lei, Y.; Hu, Z.; Chen, C.; Chen, B.; Zhu, H. Influence of rescanning parameters on selective laser melting of Ti6Al4V. *J. Manuf. Process.* **2022**, *82*, 530–542. [CrossRef]
16. Chen, Z.; Wu, X.; Tomus, D.; Davies, C.H. Surface roughness of selective laser melted Ti-6Al-4V alloy components. *Addit. Manuf.* **2018**, *21*, 91–103. [CrossRef]
17. Feng, Y.; Ma, H.; Ge, X. Computer evaluation of surface roughness parameters based on Origin. *Hebei J. Ind. Sci. Technol.* **2014**, *31*, 433–435. [CrossRef]
18. Wang, D.; Dou, W.; Ou, Y.; Yang, Y.; Tan, C.; Zhang, Y. Characteristics of droplet spatter behavior and process-correlated mapping model in laser powder bed fusion. *J. Mater. Res. Technol.* **2021**, *12*, 1051–1064. [CrossRef]
19. Ag, S. *Installation and Operation, The RTC 4 PC Interface Board for Real Time Control of Scan Heads and Lasers*; ScanLab: Nakuru, Kenya, 2006; pp. 16–28.
20. Strano, G.; Hao, L.; Everson, R.M.; Evans, K.E. Surface roughness analysis, modelling and prediction in selective laser melting. *J. Mater. Process. Technol.* **2013**, *213*, 589–597. [CrossRef]
21. Gusarov, A.; Kovalev, E. Model of thermal conductivity in powder beds. *Phys. Rev. B* **2009**, *80*, 024202. [CrossRef]
22. Tian, Y.; Tomus, D.; Rometsch, P.; Wu, X. Influences of processing parameters on surface roughness of Hastelloy X produced by selective laser melting. *Addit. Manuf.* **2017**, *13*, 103–112. [CrossRef]
23. Snyder, J.C.; Thole, K.A. Understanding laser powder bed fusion surface roughness. *J. Manuf. Sci. Eng.* **2020**, *142*, 071003. [CrossRef]
24. Temmler, A.; Comiotto, M.; Ross, I.; Kuepper, M.; Liu, D.; Poprawe, R. Surface structuring by laser remelting of 1.2379 (D2) for cold forging tools in automotive applications. *J. Laser Appl.* **2019**, *31*, 022017. [CrossRef]
25. Ramos, J.A.; Bourell, D.L.; Beaman, J.J. Surface characterization of laser polished indirect-SLS parts. In Proceedings of the 2002 International Solid Freeform Fabrication Symposium, Austin, TX, USA, 5–7 August 2002. [CrossRef]
26. Sih, S.S.; Barlow, J.W. The prediction of the emissivity and thermal conductivity of powder beds. *Part. Sci. Technol.* **2004**, *22*, 427–440. [CrossRef]
27. Shi, W.; Wang, P.; Liu, Y.; Han, G. Experiment of process strategy of selective laser melting forming metal nonhorizontal overhanging structure. *Metals* **2019**, *9*, 385. [CrossRef]
28. Wan, L.; Xia, Z.; Song, Y.; Zhang, X.; Liu, F.; Fu, G.; Shi, S. Parameter optimization of selective laser melting fabricated titanium alloy using skin-core and triple contour scanning strategy. *J. Laser Appl.* **2020**, *32*, 042001. [CrossRef]